Materials Research Bulletin 83 (2016) 225–229

Contents lists available at ScienceDirect

Materials Research Bulletin

journal homepage: www.elsevier.com/locate/matresbu

Microwave-assisted hydrothermal synthesis of $NH_4V_3O_8$ microcrystals with controllable morphology

G.S. Zakharova[a,b], A. Ottmann[b,*], B. Ehrstein[b], R. Klingeler[b,c]

[a] Institute of Solid State Chemistry, Ural Division, Russian Academy of Sciences, Pervomaiskaya ul. 91, Yekaterinburg 620990, Russia
[b] Kirchhoff Institute of Physics, Heidelberg University, INF 227, 69120 Heidelberg, Germany
[c] Centre for Advanced Materials, Heidelberg University, INF 225, 69120 Heidelberg, Germany

ARTICLE INFO

Article history:
Received 24 May 2016
Accepted 6 June 2016
Available online 7 June 2016

Keywords:
A. Inorganic compounds
A. Layered compounds
B. Chemical synthesis
D. Crystal structure
D. Electrochemical properties

ABSTRACT

Water-free $NH_4V_3O_8$ microcrystals have been successfully synthesized by a microwave-assisted hydrothermal synthesis method. The products were characterized by means of X-ray diffraction, scanning electron microscopy, Fourier transform infrared spectroscopy, thermal gravimetric analysis, cyclic voltammetry, and galvanostatic cycling. The results show phase-pure products whose particle size and morphology can be tailored by varying the reaction conditions temperature, time, and initial pH value. For instance, at low pH (2.5–3) flower-like agglomerates with primary particles of 20–30 μm length are found, while at pH 5.5 single microplates with hexagonal outline (30–40 μm) prevail. The electrochemical studies show reversible lithium de-/intercalation into the layered $NH_4V_3O_8$ host structures with a maximum initial discharge capacity of 378 mA h g^{-1} at 10 mA g^{-1}. However, there is no clear effect of the materials' morphology on their electrochemical performance.

1. Introduction

Secondary lithium batteries using a lithium-containing metal oxide as the active material of its cathode and a carbonaceous anode material have been widely used in portable electronics. $LiCoO_2$ is the principal cathode material for commercial application in Li-ion batteries [1–3]. However, it suffers from many disadvantages such as toxicity, high cost and irreversibility at elevated temperatures. Compounds based on vanadium oxides have been identified as promising alternative host structures for lithium intercalation [4,5]. Due to the wide range of oxidation states of vanadium from +2 up to +5 they carry the potential to accommodate several Li-ions per formula unit [6,7]. Among these compounds, lithium trivanadate LiV_3O_8 is one of the most studied materials for application in Li-ion batteries as it shows high specific capacity and good structural stability [7–9]. Liu et al. [10] fabricated LiV_3O_8 which demonstrated a superior insertion capacity of 347 mAh g^{-1} (3.7 Li^+/f.u.) with excellent cycling stability. However, the electrochemical performance of LiV_3O_8 strongly depends on the synthesis conditions and on post-synthesis thermal treatment, and exhibits poor rate performance [11,12]. Replacing Li^+ by other cations with larger ionic radii, such as NH_4^+ or Na^+, but preserving the monoclinic structure, yields more stable cathode materials for Li-ion batteries, e.g. $NH_4V_3O_8$ [13]. Exemplarily, Cao et al. [14] showed that $NH_4V_3O_8$ with rod-like morphology exhibits a maximum discharge capacity of 238 mAh g^{-1} at 15 mA g^{-1} with a capacity retention of 91% after 30 cycles. As one way to further improve the electrochemical performance, Wang et al. [15] found that modifying $NH_4V_3O_8$ with carbon nanotubes leads to a maximum discharge capacity of 359 mA h g^{-1} at 30 mA g^{-1} with good cycling stability as well.

Various methods have been developed to synthesize ammonium trivanadate $NH_4V_3O_8$. The traditional method is to use raw NH_4VO_3 as vanadium source, and a mineral acid (HCl or H_2SO_4) to adjust the initial pH value and to accomplish an acid hydrolysis [16,17]. Hydrothermal synthesis is a more efficient method to produce $NH_4V_3O_8$ [18]. One benefit is the variety of additional agents (sodium dodecyl sulfonate, sodium dodecyl benzene sulfonate, urea) which can be used to obtain different morphologies and, e.g., nano-scaled materials [13,19,20]. Recently, microwave-assisted routes have been widely used to synthesize nanoparticles of various oxide compounds [21–23], also in the case of $NH_4V_3O_8$ [24,25]. In comparison to the conventional hydrothermal method, microwave synthesis is faster, and more energy efficient, while allowing to control the size and shape of the obtained nano- and micro-structures [26,27].

* Corresponding author.
E-mail address: alex.ottmann@kip.uni-heidelberg.de (A. Ottmann).

http://dx.doi.org/10.1016/j.materresbull.2016.06.010
0025-5408/

In the present study, we report a simple microwave-assisted method to produce ammonium trivanadate powders. The influence of the preparation conditions on the morphology, size and electrochemical properties of $NH_4V_3O_8$ are examined in detail.

2. Experimental

Ammonium metavanadate (NH_4VO_3) and concentrated acetic acid were utilized for the synthesis, which proceeds as follows: 40 mg of NH_4VO_3 (Sigma–Aldrich) was first dissolved in 40 ml of deionized water to form a clear yellow solution. The desired amount of acetic acid (VWR Chemicals) (corresponding to a final pH value between 2.5 and 5.0) was added dropwise under stirring to the solution. The obtained solution was poured into a sealed glass vial and then transferred into a microwave reactor (Monowave 300, Anton Parr). Within a ramping time of 10 min the vial was heated to a fixed temperature (140, 160, 180, 200, or 220 °C) and held at this temperature for different periods of time. The dwell time was changed between 0.5 min and 20 min. The products were separated by centrifugation and washed with deionized water several times. For the purpose of comparison, $NH_4V_3O_8$ microcrystals were also prepared by conventional hydrothermal heating in an autoclave according to [18].

X-Ray diffraction (XRD) patterns were obtained from a Shimadzu XRD–7000 S using Cu Kα (λ = 1.541 Å) radiation with a step size of $\Delta 2\theta = 0.02^\circ$. The SEM pictures were taken on a ZEISS LEO 1530 scanning electron microscope. Transmission electron microscopy (TEM) images and selected area electron diffraction (SAED) patterns were obtained by means of a JEOL JEM–2100 F STEM/EDS electron microscope. FT-IR spectra were recorded using a Spectrum One B (Perkin Elmer). Differential scanning calorimetry (DSC-TG) was performed on a DSC Q10 (TA Instruments) while heating the samples with 10 K min^{-1} from room temperature up to 800 °C in air. The specific surface area and pore volume of the samples was measured by a surface area and porosity analyzer (Gemine VII, Micromeritics).

For electrochemical characterization (cf. [28]), pristine $NH_4V_3O_8$ powder was stirred overnight with 5 wt% polyvinyldeneflourid binder (Solvay Plastics) and 15 wt% carbon black (Timcal) in *N*-methyl-2-pyrrolidone (Sigma-Aldrich). The resulting slurry was spread on Al-meshes, dried at ~80 °C under vacuum, mechanically pressed and dried again. The Swagelok-type two-electrode cells were assembled in an Ar-atmosphere glove box. The working electrode and a lithium metal foil counter electrode were separated by two layers of glass fiber separator (Whatman GF/D). The electrolyte was 1 mol/l $LiPF_6$ in a mixture of ethylene carbonate and dimethyl carbonate (Merck Electrolyte LP30). Electrochemical measurements by means of cyclic voltammetry and galvanostatic cycling with potential limitation (GCPL) were carried out by a VMP3 Potentiostat System (BioLogic) in the potential range of 1.0–4.0 V vs. $Li^{0/+}$ at constant temperature (25 °C).

3. Results and discussion

The structure of the as-prepared microcrystals was characterized by means of X-ray powder diffraction. In Fig. 1, exemplary XRD patterns of two samples synthesized by the microwave-assisted route (MW), representing the lowest and the highest applied synthesis temperature (140 °C (MW1)/220 °C (MW2) for 15/20 min, pH 4), are shown in comparison to a conventionally synthesized one (AC) (140 °C for 48 h, pH 4). All diffraction peaks can be indexed in the monoclinic lattice system with space group *P 21/m* and correspond to $NH_4V_3O_8$ (JCPDS card no. 088-1473 [29]). Lattice parameters were determined by means of full-profile analyses with the FullProf Suite. The MW1 sample exhibits

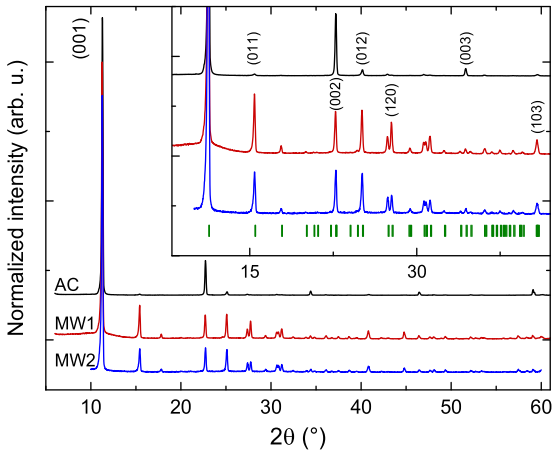

Fig. 1. XRD patterns of $NH_4V_3O_8$ prepared by conventional hydrothermal treatment (AC; black line), and the microwave-assisted method (MW1/2; red line: 140 °C, blue line: 220 °C). Inset: Detail of the data with Bragg positions according to JCPDS card no. 088-1473 [29], marked in green. (For interpretation of the references to color in this figure legend, the reader is referred to the web version of this article.)

a = 4.989(4) Å, b = 8.407(5) Å, c = 7.853(4) Å, and β = 96.41(5)° which is in agreement with the lattice constants of the AC one, synthesized under the same conditions [28]. High purity of all samples is indicated by the absence of any characteristic impurity peaks (also see supporting information Fig. S1). The patterns of the MW and the AC $NH_4V_3O_8$ samples however feature one obvious difference, which is the relative intensity of the (00*l*) Bragg peaks. The AC sample shows in comparison with other reflections much more pronounced (001), (002) and (003) peaks, e.g. the intensity ratio $I_{(001)}/I_{(011)}$ is more than 25 times greater than that of the MW samples. This observation can be attributed to preferred orientation of the single microcrystals of the AC sample (cf. Fig. 2d) as opposed to the more randomly oriented agglomerates (Fig. 2b/e) which result from the microwave-assisted synthesis.

The morphology of the as-prepared $NH_4V_3O_8$ materials was examined by SEM (Fig. 2). The impact of the synthesis conditions (pH value, reaction temperature, heating duration) on the product's morphology was studied by changing one reaction parameter while the other conditions were kept constant. It turned out that the pH value of the precursor solution is the most crucial factor for the morphology of the hydrothermally synthesized $NH_4V_3O_8$. In case of the microwave-assisted hydrothermal treatment the pH value was varied from 2.5 to 5.5, while the temperature was always set to 140 °C for 20 min. When the pH value equals 2.5–3.0, the dominant microstructures are flower-like three-dimensional (3D) agglomerates composed of many leaf-like microsheets with lengths of 20–30 μm (Fig. 2a). The inset (Fig. 2a) reveals that the thickness of the leaf-like particles is in the range of 0.5–1.5 μm and that the width is around 10 μm. These microleaves alternatingly overlie each other similar to petals forming a flower. Upon increasing the pH value from 3.0 to 5.5, the morphology gradually transforms from rather loosely aggregated microleaves to single microplates with hexagonal outline (Fig. 2b-c). The primary particles in the material obtained at pH 4 (140 °C) exhibit plate-like shape with 0.5–1.5 μm thickness, 10–30 μm width and 10–60 μm length. Some of the microplates can still be found in agglomerates similar to a flower with "open petals" (Fig. 2b). Note, that the exemplarily obtained selected area electron diffraction (SAED) pattern (see Fig. S2) confirms the single crystalline nature of the primary particles in the as-prepared $NH_4V_3O_8$ sample. At pH 5, regular hexagonal microplates are observed (Fig. 2c). The dimensions of these hexagons are in the range of 30–40 μm, and with 140–700 nm they are thinner than the primary particles

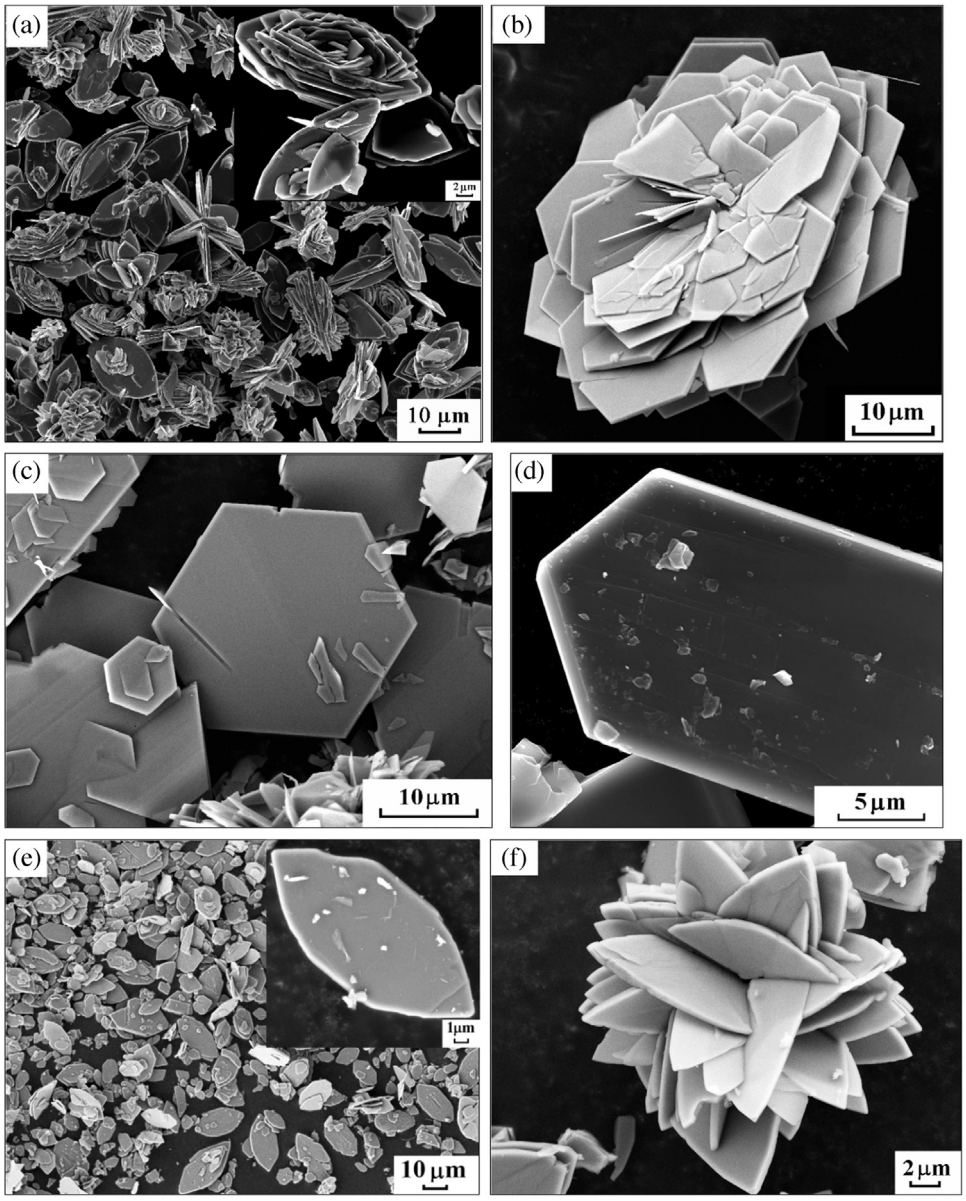

Fig. 2. SEM images of $NH_4V_3O_8$ synthesized by (a–c, e, f) microwave-assisted method and (d) conventional hydrothermal treatment under different conditions: (a) pH 2.5, 140 °C for 20 min, (b) pH 4.0, 140 °C for 20 min, (c) pH 5.0, 140 °C for 20 min, (d) pH 4, 160 °C for 48 h, (e) pH 2.5, 220 °C for 0.5 min, (f) pH 2.5, 140 °C for 1 min.

found at lower pH. The observed differences in morphology can be ascribed to different nucleation rates of $NH_4V_3O_8$ induced by both different pH values (i.e. H^+ concentration) and different oxidation states of the vanadium ions in the reaction solution [16]. In comparison, the average lengths and thicknesses of the $NH_4V_3O_8$ microplates synthesized by conventional hydrothermal treatment at pH 4.5–5.5 (Fig. 2d) are larger than those of the MW materials. The AC particles show lengths of 60–80 μm, widths of 30–60 μm, and thicknesses ranging from 1.1 to 2.3 μm.

Varying the temperature of the microwave heating from 140 °C up to 220 °C at fixed pH = 4 and dwell time (20 min) hardly changes the morphology but reduces the particle size from 30 to 60 μm (140 °C) to 20–40 μm (220 °C). Concomitantly, the degree of agglomeration decreases as well. Furthermore, it was found that the variation of the dwell time affects the size of the $NH_4V_3O_8$ microcrystals. The corresponding experiments were carried out at pH 2.5 and at temperatures of 140 °C and 220 °C. The shortest dwell time of 0.5 min at 220 °C yields mainly leaf-like structures with a length of 25–40 μm, width of 15–20 μm, and thickness of 400–900 nm (Fig. 2e). Prolonging the reaction time to 1 min (Fig. 2f) and 20 min (Fig. 2a), respectively, leads to single leaves crossing each other and further to the flower-like structures described above. At the same time, the thickness and the width of the microleaves increase while the length does not change.

The FT-IR spectrum of $NH_4V_3O_8$, synthesized at pH 4 and 140 °C for 20 min inside the microwave reactor, is shown in Fig. 3 in comparison to the data of a conventionally synthesized one (pH 4, 160 °C for 48 h; cf. Ref. [18]). In case of the MW sample, there are several distinct absorption bands at 3217, 1404, 1006, 966, 737, 597, 528 and 452 cm^{-1}, which can be assigned to different excitations of the ammonium trivanadate structure [30]. The bands at 1006 cm^{-1} and 966 cm^{-1} are assigned to V=O symmetric stretching vibrations in the distorted octahedron and the distorted square pyramids, respectively. The band at 737 cm^{-1} corresponds to an asymmetric stretching vibration of the V—O—V bridges. The absorption band centered around 528 cm^{-1} is due to symmetric stretching vibrations of V—O—V bonds. The band at 1404 cm^{-1} is attributed to symmetric bending vibrations of the NH_4^+ group. The

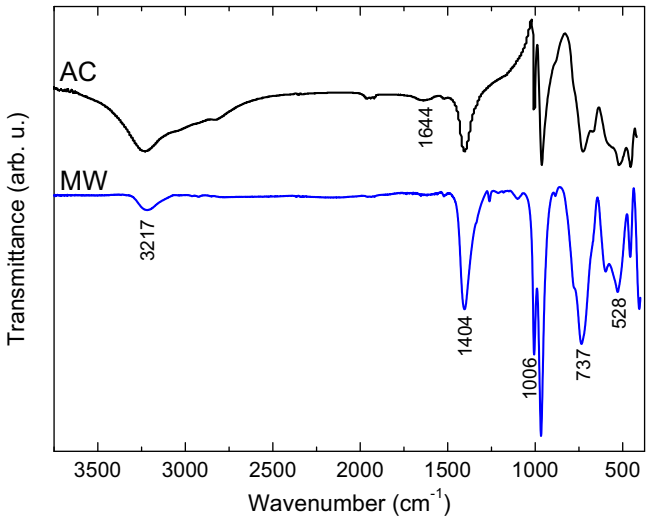

Fig. 3. FT-IR spectra of $NH_4V_3O_8$ synthesized by microwave-assisted method at pH 2.5, 220 °C for 0.5 min (MW) and conventional hydrothermal treatment at pH 4, 160 °C for 48 h (AC).

corresponding asymmetric stretching vibrations are reflected in the peak at 3217 cm^{-1} [31]. The pronounced broadening of this stretching band indicates the presence of a dense network of hydrogen bonds [18]. The AC sample shows very similar absorption bands, albeit the intensities of the bands differ. The broad absorption band around 1644 cm^{-1} indicating the presence of crystal water [16,18] is absent in case of the microwave-assisted route, which provides evidence for the pristine material being water-free $NH_4V_3O_8$.

In order to confirm the fabrication of water-free $NH_4V_3O_8$ by microwave-assisted hydrothermal synthesis and to determine the thermal stability of the sample, DSC-TG analysis of the as-prepared material (pH 3.0, 160 °C for 20 min) was carried out (see Fig. 4). There is an endothermic peak at 334 °C with an integrated weight loss of about 8.73%, which can be attributed to the decomposition of $NH_4V_3O_8$ according to the following equation:

$$2NH_4V_3O_8 \rightarrow 3\,V_2O_5 + 2NH_3\uparrow + H_2O \quad (1)$$

The endothermic feature at 682 °C in the DSC curve demonstrates the melting process of vanadium pentoxide.

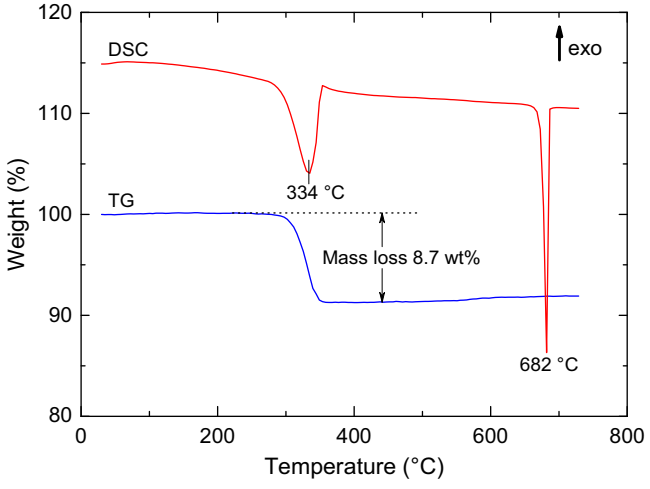

Fig. 4. DSC and TG scans of $NH_4V_3O_8$ powder synthesized by microwave-assisted method at pH 3.0, 160 °C for 20 min (initial sample mass: 10.643 mg).

During the microwave-assisted hydrothermal process, NH_4VO_3 reacts with acetic acid to form ammonium trivanadate molecules in the same way as during the conventional heating [18]:

$$3NH_4VO_3 + CH_3COOH \rightarrow NH_4V_3O_8 + NH_3 + CH_3COONH_4 + H_2O \quad (2)$$

Comparing the two synthesis methods, the microwave-assisted one allows to obtain phase-pure crystalline $NH_4V_3O_8$ powder in shorter time and with smaller particle dimensions.

The electrochemical performance of two MW samples with different morphologies, i.e. primary particles with leaf-like (MW2, Fig. 2e) and hexagonal-shaped (MW1, Fig. 2c) outline, respectively, was studied by means of cyclic voltammetry and galvanostatic cycling, both in the range of 1.0–4.0 V vs. $Li^{0/+}$. The results are discussed in comparison to those of conventionally synthesized microbelts (Fig. 2d), which were reported in detail elsewhere [28] (Fig. 5). The three samples under study exhibit different specific surface areas of 1.8(1) m^2/g (AC), 2.6(1) (MW1), and 11(1) m^2/g (MW2). The cyclic voltammograms (CV) (Fig. 5a) show that all samples exhibit the same redox features with two dominant peaks around 1.6 V (reduction) and 3 V (oxidation), respectively. The redox activity originates from the $V^{5+/4+}$ and $V^{4+/3+}$ couples, and is associated with the intercalation and deintercalation of Li^+-ions into the layered $NH_4V_3O_8$ structure [13,28]. The MW2 sample features noticeably higher current intensities in the CV as compared to the other materials, which can be ascribed to the

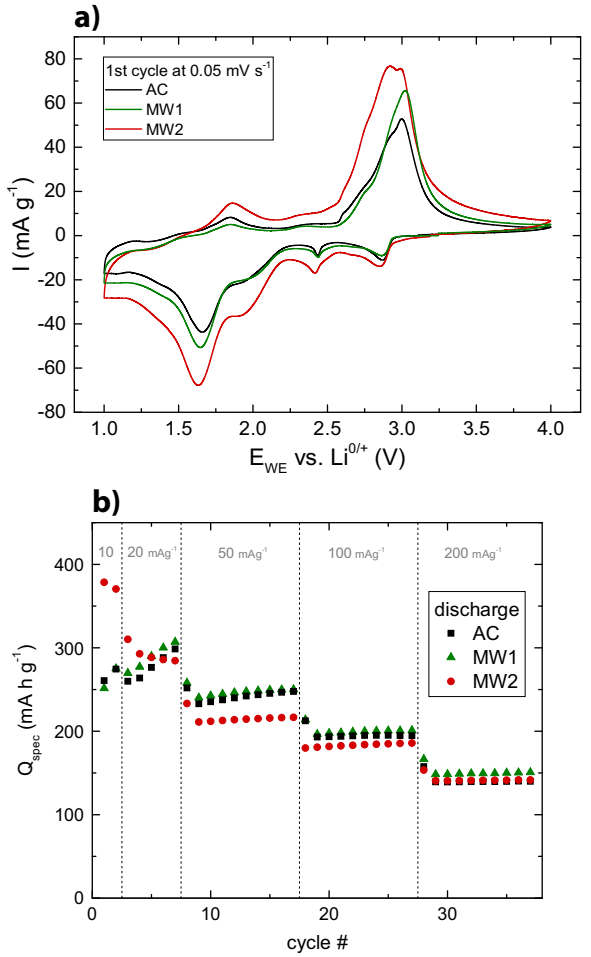

Fig. 5. (a) Cyclic voltammograms of MW1 (green line; pH 5.5, 140 °C for 20 min), MW2 (red line; pH 2.5, 220 °C for 0.5 min), and AC (black line; pH 4, 140 °C for 48 h) materials. (b) Discharge capacities for the same samples at various current rates. (For interpretation of the references to color in this figure legend, the reader is referred to the web version of this article.)

greater active surface area of the MW2 sample. Consequently, this sample also shows the highest initial discharge capacity of 378 mA h g^{-1} at 10 mA g^{-1}. This corresponds to the intercalation of 4.2 Li^+/f.u., compared to 261 mA h g^{-1} (2.9 Li^+/f.u.) in case of the AC microbelts. However, during the further course of the GCPL with increasing charge/discharge rates of 20, 50, 100 and 200 mA h g^{-1}, respectively, the capacities of the three materials converge and no significant difference can be observed anymore. In contrast to the other samples, the MW2 sample shows decreasing capacities during the first seven cycles which could be caused by irreversible structure change/damage due to too deep discharge (Li^+ intercalation). In summary, no clear dependence of the overall electrochemical performance on either the sample morphology or the synthesis route (MW vs. AC) is observed. One has to conclude that although morphology and particle size have been widely varied in the materials studied here, none of the modifications is crucial for the electrochemical performance.

6. Conclusions

Morphology-controlled synthesis of $NH_4V_3O_8$ microcrystals was achieved via a microwave-assisted hydrothermal approach with short reaction times (<30 min). The reaction conditions, in particular the pH value of the precursor solution, show a considerable impact on the particle size and morphology of the synthesized powder materials. The morphologies can be varied from flower-like agglomerates (pH 2.5, 140 °C for 20 min) to single hexagonal-shaped platelets (pH 5.5, 140 °C for 20 min) with particle dimensions in the order of 10 μm. XRD, DSC-TG and FT-IR measurements confirm the phase purity of the samples, and the absence of characteristic absorption bands in the FT-IR spectrum indicates that the pristine $NH_4V_3O_8$ is water-free. Electrochemical characterization by means of CV and GCPL reveals typical Li^+ de-/intercalation activity attributed to the $V^{5+/4+}$ and $V^{4+/3+}$ redox couples with a maximum initial discharge capacity of 378 mA h g^{-1} at 10 mA g^{-1}.

Acknowledgements

This work was supported by the Ministry of Science and Education of Russian Federation (unique project identifier RFMEF161314X0002) and by the CleanTech-Initiative of the Baden-Württemberg-Stiftung (Project CT3: Nanostorage). G.S.Z acknowledges support by the Excellence Initiative of the German Federal Government and States. A.O. acknowledges support by the IMPRS-QD.

Appendix A. Supplementary data

Supplementary data associated with this article can be found, in the online version, at http://dx.doi.org/10.1016/j.materresbull.2016.06.010.

References

[1] Y. Wang, G. Cao, Developments in nanostructured cathode materials for high-performance lithium-ion batteries, Adv. Mater. 20 (2008) 2251–2269.
[2] B. Scrosati, J. Garche, Lithium batteries: status, prospects and future, J. Power Sources 195 (2010) 2419–2430.
[3] J.W. Fergus, Recent developments in cathode materials for lithium ion batteries, J. Power Sources 195 (2010) 939–954.
[4] Q.-H. Wu, Electrochemical potential of intercalation phase: Li/V2O5 system, Applied Surf. Sci. 253 (2006) 1713–1716.
[5] A. Shimizu, T. Tsumura, M. Inagaki, Electrochemical intercalation of lithium into V2O5: effect of host materials, Solid State Ionics 63–65 (1993) 479–483.
[6] C. Wu, Y. Xie, Promising vanadium oxide and hydroxide nanostructures: from energy storage to energy saving, Energy Environ. Sci. 3 (2010) 1191–1206.
[7] N.A. Chernova, M. Roppolo, A.C. Dillon, M.S. Whittingham, Layered vanadium and molybdenum oxides: batteries and electrochromics, J. Mater. Chem. 19 (2009) 2526–2552.
[8] N. Kumagai, A. Yu, Ultrasonically treated LiV3O8 as a cathode material for secondary lithium batteries, J. Electrochem. Soc. 144 (1997) 830–835.
[9] J. Dai, S.F.Y. Li, Z. Gao, K.S. Siow, Low-temperature synthesized LiV3O8 as a cathode material for rechargeable lithum batteries, J. Electrochem. Soc. 145 (1998) 3057–3062.
[10] H. Liu, Y. Wang, W. Yang, H. Zhou, A large capacity of LiV3O8 cathode material for rechargeable lithium-based batteries, Electrochim. Acta 56 (2011) 1392–1398.
[11] S.H. Ju, Y.C. Kang, Effect of preparation temperature on the morphology, crystal structure and electrochemical properties of LiV3O8 powders prepared by spray pyrolysis, Mater. Chem. Phys. 126 (2011) 133–137.
[12] J. Xu, H. Zhang, T. Zhang, Q. Pan, Y. Gui, Influence of heat-treatment temperature on crystal structure, morphology and electrochemical properties of LiV3O8 prepared by hydrothermal reaction, J. Alloys Compd. 467 (2009) 327–331.
[13] H. Wang, K. Huang, S. Liu, C. Huang, W. Wang, Y. Ren, Electrochemical property of NH4V3O8·0.2H2O flakes prepared by surfactant assisted hydrothermal method, J. Power Sources 196 (2011) 788–792.
[14] S.-S. Cao, J.-F. Huang, H.-B. Ouyang, L.-Y. Cao, J.-Y. Li, J.-P. Wu, A simple method to prepare NH4V3O8 nanorods as cathode material for Li-ion batteries, Mater. Lett. 126 (2014) 20–23.
[15] H. Wang, K. Huang, Y. Ren, X. Huang, S. Liu, W. Wang, NH4V3O8/carbon nanotubes composite cathode material with high capacity and good rate capability, J. Power Sources 196 (2011) 9786–9791.
[16] L.Q. Mai, C.S. Lao, B. Hu, J. Zhou, Y.Y. Qi, W. Chen, E.D. Gu, Z.L. Wang, Synthesis and electrical transport of single-crystal NH4V3O8 nanobelts, J. Phys. Chem. B 110 (2006) 18138–18141.
[17] N. Wang, W. Chen, L. Mai, Y. Dai, Selected-control hydrothermal synthesis and formation mechanism of 1D ammonium vanadate, J. Solid State Chem. 181 (2008) 652–657.
[18] G.S. Zakharova, C. Täschner, T. Kolb, C. Jähne, A. Leonhardt, B. Büchner, R. Klingeler, Morphology controlled NH4V3O8 microcrystals by hydrothermal synthesis, Dalton Trans. 42 (2013) 4897–4902.
[19] H. Wang, Y. Ren, W. Wang, X. Huang, K. Huang, Y. Wang, S. Liu, NH4V3O8 nanorod as a high performance cathode material for rechargeable Li-ion batteries, J. Power Sources 199 (2012) 315–321.
[20] H.-K. Park, G. Kim, Ammonium hexavanadate nanorods prepared by homogeneous precipitation using urea as cathodes for lithium batteries, Solid State Ionics 181 (2010) 311–314.
[21] J.-M. Li, K.-H. Chang, T.-H. Wu, C.-C. Hu, Microwave-assisted hydrothermal synthesis of vanadium oxides for Li-ion supercapacitors: the influences of Li-ion doping and crystallinity on the capacitive performances, J. Power Sources 224 (2013) 59–65.
[22] S. Komarneni, R.K. Rajha, H. Katsuki, Microwave-hydrothermal processing of titanium dioxide, Mater. Chem. Phys. 61 (1999) 50–54.
[23] C. Neef, C. Jähne, H.-P. Meyer, R. Klingeler, Morphology and agglomeration control of LiMnPO4 micro- and nanocrystals, Langmuir 29 (2013) 8054–8060.
[24] S. Cao, J. Huang, X. Zhanwei, L. Jiayin, O. Haibo, C. Liyun, Z. Lei, Influence of microwave heating on the structure and electrochemical property of NH4V3O8 cathode material for lithium ion batteries, Ceram. Int. 41 (2015) 6747–6752.
[25] S. Cao, J. Huang, Y. Cheng, R. Li, J. Li, Z. Xu, H. Ouyang, L. Cao, J. Wu, Facile synthesis of ultralong NH4V3O8 nanobelts cathode material for lithium ion battery, J. Electroanal.Chem. 752 (2015) 12–16.
[26] K. Chen, Y.D. Noh, R.R. Patel, W. Huang, J. Ma, K. Li, S. Komarneni, D. Xue, Microwave- or conventional-hydrothermal synthesis of Co-based materials for electrochemical energy storage, Ceram. Int. 40 (2014) 8183–8188.
[27] I. Bilecka, M. Niederberger, Microwave chemistry for inorganic nanomaterials synthesis, Nanoscale 2 (2010) 1358–1374.
[28] A. Ottmann, G.S. Zakharova, B. Ehrstein, R. Klingeler, Electrochemical performance of single crystal belt-like NH4V3O8 as cathode material for lithium-ion batteries, Electrochim. Acta 174 (2015) 682–687.
[29] S.D. Huang, Y. Shan, NH4V3O8: a novel sinusoidal layered compound formed by the cation templating effect, Chem. Commun. (1998) 1069–1070.
[30] B. Azambre, M.J. Hudson, O. Heintz, Topotactic redox reactions of copper(ii) and iron(iii) salts within VOx nanotubes, J. Mater. Chem. 13 (2003) 385–393.
[31] G. Madhurambal, S.C. Mojumdar, S. Hariharan, P. Ramasamy, TG, DTA, FTIR and Raman spectral analysis of Zna/Mgb ammonium sulfate mixed crystals, J. Therm. Anal. Calorim. 78 (2004) 125–133.